Quantum Monte Carlo tunneling from quantum chemistry to quantum annealing

Guglielmo Mazzola,[1,*] Vadim N. Smelyanskiy,[2] and Matthias Troyer[1,3]
[1]*Theoretische Physik, ETH Zurich, 8093 Zurich, Switzerland*
[2]*Google, Venice, California 90291, USA*
[3]*Quantum Architectures and Computation Group, Station Q, Microsoft Research, Redmond, Washington 98052, USA*
(Received 13 April 2017; revised manuscript received 21 August 2017; published 11 October 2017)

Quantum tunneling is ubiquitous across different fields, from quantum chemical reactions and magnetic materials to quantum simulators and quantum computers. While simulating the real-time quantum dynamics of tunneling is infeasible for high-dimensional systems, quantum tunneling also shows up in quantum Monte Carlo (QMC) simulations, which aim to simulate quantum statistics with resources growing only polynomially with the system size. Here we extend the recent results obtained for quantum spin models [Phys. Rev. Lett. **117**, 180402 (2016)], and we study continuous-variable models for proton transfer reactions. We demonstrate that QMC simulations efficiently recover the scaling of ground-state tunneling rates due to the existence of an instanton path, which always connects the reactant state with the product. We discuss the implications of our results in the context of quantum chemical reactions and quantum annealing, where quantum tunneling is expected to be a valuable resource for solving combinatorial optimization problems.

DOI: 10.1103/PhysRevB.96.134305

I. INTRODUCTION

Quantum-mechanical tunneling (QMT) plays a fundamental role in a broad range of disciplines, from chemistry and physics to quantum computing. QMT can be observed in chemical reactions [1–4], and it affects the description of water and related aqueous system at room temperature [5,6]. It is essential for understanding—even at the qualitative level—the phase diagrams of correlated materials, such as dense hydrogen, which is the simplest condensed-matter system [7–10].

QMT can also be engineered in quantum annealers [11,12] to solve optimization problems using quantum effects [13–17]. Here, quantum tunneling could provide a large advantage [18], particularly when the energy landscapes display tall but thin barriers, which are easier to tunnel through quantum mechanically rather than to climb over by means of thermally activated rare events, whose frequency is exponentially suppressed as the height of the barrier increases.

In general, simulating real-time quantum dynamics requires the direct integration of the time-dependent Schrödinger equation. This is a formidable task as the Hilbert space of the systems grows exponentially with the number of constituents, which makes the unitary evolution of a quantum system only possible for fairly small problem sizes, on the order of 40–50 spins. The characterization of quantum dynamics simplifies when it is dominated by tunneling events. In this case, the useful quantities we want to predict are the transition rate between the initial and final state (e.g., reactants and product in chemical reactions) and the pathway of the transition.

For simplicity, let us first consider tunneling in a deep double-well system, well described by the lowest two eigenstates of the unperturbed tunneling system, $|\psi_0\rangle$ and $|\psi_1\rangle$, which can be expressed as linear combinations of the degenerate states $|\psi_L\rangle$ and $|\psi_R\rangle$, localized, respectively, in the left and right well (see Fig. 1). The isolated system exhibits characteristic oscillatory behavior between the unperturbed states, $|\psi_L\rangle$ and $|\psi_R\rangle$, under the action of the Hamiltonian H, with frequency proportional to the tunneling matrix element $\langle\psi_L|H|\psi_R\rangle = \Delta/2$.

Coherence is easily destroyed by the presence of external noise, as is the case in the proton transfer reactions and in quantum annealing (QA). Coupling to an environment can then stop the oscillatory behavior, and the transition rate is given by the *incoherent* tunneling rate, proportional to Δ^2 [19]. This is also the relevant tunneling rate in the adiabatic evolution of quantum annealing, where the annealing time must scale as Δ^{-2} in order to avoid Landau-Zener diabatic transitions from the ground state to the first excited state [13,14].

QMT also appears in quantum Monte Carlo (QMC) simulations, which can be efficient for quantum many-body problems without a sign problem (i.e., that the system should obey bosonic statistics or distinguishable particles). In this case (in the absence of exponentially large equilibration times, which can sometimes be present near phase transitions and at very low temperatures), the computational effort to describe equilibrium statistics scales polynomially with the system size. Path integral Monte Carlo (PIMC) has been successfully applied to a broad range of continuum and lattice models. In particular, PIMC simulations [20,21] have addressed problems in which QMT is important, such as proton delocalization in water [22,23], hydrogen [24], and QA [25,26].

PIMC is based on the path integral formalism of quantum mechanics, and it samples the density matrix corresponding to the quantum Hamiltonian H by means of a classical Hamiltonian $H_{\rm cl}$ on an extended system having an additional dimension, the *imaginary-time* direction. The original quantum system is thus mapped into a classical one, which can be simulated by standard Monte Carlo sampling.

Although QMC techniques are rigorously derived to describe equilibrium properties, we show here that equilibrium PIMC simulations also provide important dynamical quantities, and in particular the quantum tunneling rate. In Ref. [27], we have studied tunneling events in a ferromagnetic Ising model. The Ising ferromagnet can be described by an effective

*gmazzola@phys.ethz.ch

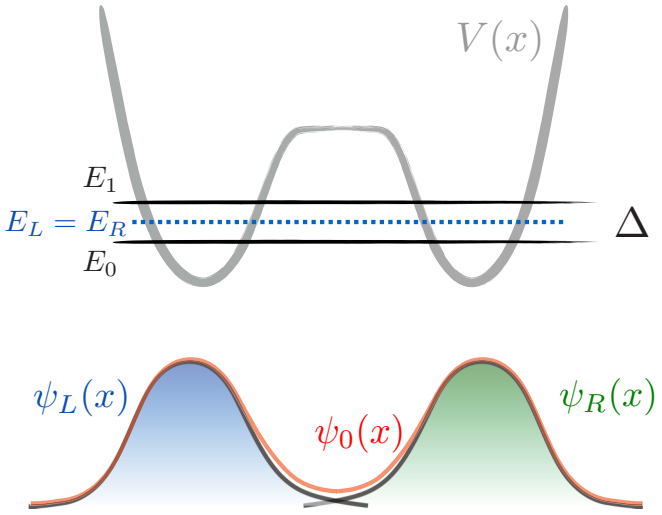

FIG. 1. Illustration of a double-well potential energy $V(x)$ and energy levels. The degenerate levels E_L and E_R correspond to the localized states $|\psi_L\rangle$ (blue) and $|\psi_R\rangle$ (green). The degeneracy is lifted by the linear combination of localized states that produce the true eigenstates $\psi_0 = 1/\sqrt{2}(|\psi_L\rangle + |\psi_R\rangle)$ (red curve) and $\psi_1 = 1/\sqrt{2}(|\psi_L\rangle - |\psi_R\rangle)$. The tunneling splitting Δ can be calculated from the overlap of the localized states.

double-well model, with the total scalar magnetization as a reaction coordinate. We have demonstrated numerically that PIMC tunneling events occur with a rate k that scales, to leading exponential order, as Δ^2—identical to the physical dynamics. We have also seen that with open boundary conditions (OBCs) in imaginary time, the tunneling rate becomes Δ, thus providing a quadratic speedup.

In this paper, we investigate the scaling relation between the PIMC tunneling rate and Δ for a broader class of problems, which are of paradigmatic importance in quantum chemistry. We explore models in which the effective one-dimensional picture of tunneling should break down [28]. Our results for continuous variables extend those for the Ising model [27], and we find that the QMC tunneling rate always follows Δ^2 scaling (or better with OBCs). We argue that this is a manifestation of a phenomenon in which QMC can efficiently simulate the tunneling splitting of the ground-state energy levels in a broad class of multidimensional systems, in all cases when the autocorrelation time of the QMC pseudodynamics remains finite (see Sec. V).

II. INSTANTONS AND QMC

A. Path integral Monte Carlo

PIMC and path integral molecular-dynamics (PIMD) techniques arose directly from the Feynman path integral formulation of quantum mechanics, and they are used to simulate thermodynamic equilibrium. To briefly introduce this approach for continuous space, we start from the expression for the partition function Z:

$$Z = \int dx \langle x|e^{-\beta H}|x\rangle, \tag{1}$$

where x is the particle position (the generalization to arbitrary dimensions is straightforward), $\beta = 1/k_B T$ is the inverse temperature, and H is the Hamiltonian of the system. Typical real-space Hamiltonians are sums of two noncommuting operators $H = \Theta + V$, where $\Theta = 1/2m\partial^2/\partial x^2$ is the kinetic operator (m being the particle mass) and $V(x)$ is the potential energy. We first notice that the operator $e^{-\beta H}$ corresponds to an evolution in imaginary time β. We use the Trotter-Suzuki approximation $e^{-\delta_\tau(\Theta+V)} \approx e^{-\delta_\tau\Theta}e^{-\delta_\tau V}$ for small δ_τ [21].

Splitting the imaginary-time evolution into P small time steps of length $\delta_\tau = \beta/P$, the path integral expression for Eq. (1) then becomes

$$Z \propto \int dx_1 dx_2 \cdots dx_P \exp \sum_{i=1}^{P} S_i, \tag{2}$$

where $S_i = K_i + U_i$ is the *action* of each step. $K_i = (x_{i-1} - x_i)^2/(2\delta_\tau/m)$ is the kinetic part and $U_i = \delta_\tau/2[V(x_{i-1} - x_i)]$ in the so-called *primitive* approximation. Notice that $x_1 = x_P$ (closed boundary conditions in imaginary time) for evaluating the trace of the density operator.

This provides an analogy between a quantum system and a classical system with an additional dimension: Eq. (2) is a classical configurational integral, and the multidimensional object $(x_1, \ldots, x_{P-1}) \equiv \mathbf{x}(\tau)$ can be viewed as a *ring polymer*, whose elements are connected by springs. Each element is labeled by its position along the imaginary-time axis, with $0 \leqslant \tau < \beta$. We refer the reader to Ref. [21] for a detailed review of path integrals. An essential feature of Eq. (2) is that the integrand is positive, and hence the distribution $\exp \sum_{i=1}^{P} S_i$ can be sampled by means of METROPOLIS Monte Carlo methods or molecular-dynamics (MD) simulations. The main difference between a pure Monte Carlo and a MD approach is that the latter samples from the canonical distribution by evolving an appropriate equation of motion, whereas the former uses stochastic Monte Carlo dynamics (see the Appendix).

B. Instantons in PIMC

Connections between exact quantum dynamics and PIMD approaches, such as centroid molecular dynamics [29] and ring polymer molecular dynamics [30], have been discussed [31–33] in the context of real-space simulations. Here we follow an alternative approach and summarize the picture of Refs. [27,34] based on the *instanton* theory of tunneling through energy barriers.

In a PIMC or PIMD simulation, one samples paths $\mathbf{x}(\tau,t)$ at each update along the simulation time axis t, and these paths are distributed according to the functional $S(\mathbf{x}(\tau))$ as in Eq. (2). We can define an underlying pseudodynamics used to sample the paths to be given by a first-order Langevin dynamics, $\partial\mathbf{x}(\tau,t)/\partial t = -\delta S/\delta\mathbf{x}(\tau,t) + \eta(\tau,t)$. In this case, the analogy between quantum statistic and classical statistical mechanics has already been worked out in the *stochastic quantization* approach in the context of quantum field theory [35]. Here, the velocity of the (deformations of) path $\partial\mathbf{x}(\tau,t)/\partial t$ is linked to the generalized force $\delta S/\delta\mathbf{x}(\tau,t)$ and a Gaussian white noise $\eta(\tau,t)$ satisfying the obvious fluctuation-dissipation relation. We can numerically integrate the discretized version of the

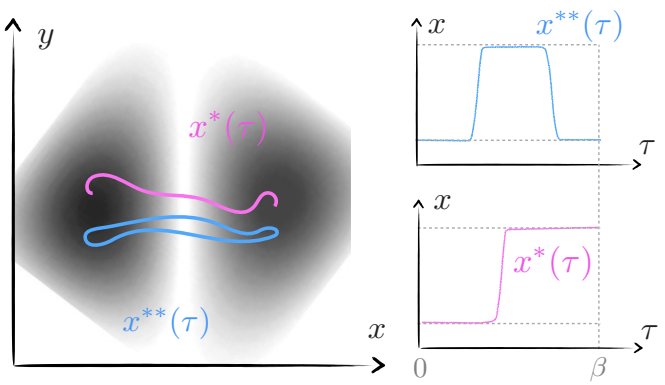

FIG. 2. Left: Illustration of the typical instantonic paths in configuration space, with PBC, $\mathbf{x}^{**}(\tau)$ (cyan), and OBC in imaginary time, $\mathbf{x}^{*}(\tau)$ (pink). These paths are transition states of the PIMC and path integral ground-state (PIGS) pseudodynamics, respectively (in the space of imaginary-time trajectories) in double-well models (sketched in the gray-scale heat map; see Fig. 6 for a more realistic example). Right: Instantonic trajectories (projected on the reaction coordinate x axis) as a function of the imaginary time τ. Notice that PIMC instantons have to cross twice the barrier to fulfill the PBC constraint.

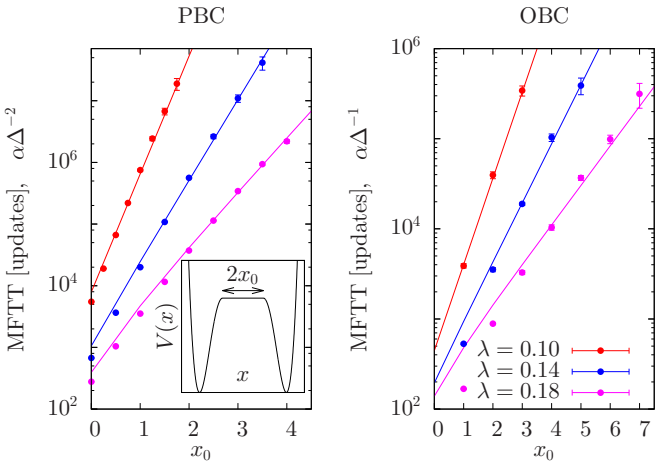

FIG. 3. Average mean first tunneling time (MFTT) with PIMC (for PBCs and OBCs) as a function of x_0 for different values of λ, at $\beta = 20$, corresponding to a temperature always much lower than the barrier height. We use a dimensionless mass parameter $m = 1/2$. The inset shows the shape of the double-well potential $V(x)$, whose barrier width (at the top) is $2x_0$. In the OBC case, deviations from the expected $1/\Delta$ behavior occur when the tunneling rate becomes larger.

equation of motion (with time step δ_t), $\mathbf{x}(\tau, t+\delta_t) = \mathbf{x}(\tau,t) - \delta_t \delta S/\delta \mathbf{x}(\tau,t) + \sqrt{2\delta_t}\mathbf{z}(\tau,t)$, where $\mathbf{z}(\tau,t)$ is a deformation path, which, after a Trotter discretization, is a vector of uniformly random distributed numbers in the range $[-1,1]$. This defines a Markov chain whose fixed point is the desired distribution, in the $\delta_t \to 0$ limit.

If the system displays two degenerate minima, then the transition state of the pseudodynamics is given by the point $\mathbf{x}_{\mathrm{TS}}(\tau)$ satisfying $\delta S(\mathbf{x}_{\mathrm{TS}}(\tau))/\delta \mathbf{x}(\tau) = 0$ with the condition that $\mathbf{x}_{\mathrm{TS}}(\tau)$ is not entirely contained in one of the attraction basins corresponding to the two minima [35–38].

Finding this transition state is generally very complicated, but in the case of a double-well potential $V(x)$ it can be done analytically. Here the dominant contribution to the integral comes from the stationary action path $\mathbf{x}^{**}(\tau)$ [determined exactly by the condition $\delta S(\mathbf{x}(\tau))/\delta \mathbf{x}(\tau) = 0$], which is called an instanton [39–41]. This trajectory in imaginary time corresponds to a particle moving in the inverted potential $-V(x)$ (see Fig. 2). Following Ref. [27], it is possible to evaluate the action S at this point, and the amplitude is given by

$$\exp\left(-S[\mathbf{x}^{*}(\tau)]\right) \propto \Delta \quad \text{(instanton)}, \tag{3}$$

where $\mathbf{x}^{*}(\tau)$ is the open trajectory that connects the two classical turning points under the barrier, near the minima. Notice that, when computing the (diagonal) density matrix $\rho(x)$, PBCs in imaginary time are required. Now the integral over the *closed* paths is dominated by the imaginary-time trajectory $\mathbf{x}^{**}(\tau)$, which moves under the start of the barrier, reaches the turning point, and returns. Therefore, the saddle-point estimation of the integral gives a *squared* tunneling amplitude

$$\exp\left(-S[\mathbf{x}^{**}(\tau)]\right) \propto \Delta^2 \quad \text{(double instanton)}, \tag{4}$$

due to the cost of creating an instanton and an anti-instanton (see Fig. 2). Returning to the PIMD pseudodynamics, according to Kramers theory [42], the escape rate is $k \propto e^{-S(\mathbf{x}_{\mathrm{TS}})}$, and therefore $k \propto \Delta^2$ if standard closed path integrals are used, whereas $k \propto \Delta$ if the paths are opened. In Sec. III we extend the study of Ref. [27] and demonstrate that the quadratic speedup in the tunneling rate in the case of open boundary path integrals holds also in multidimensional continuous-space problems.

III. ONE-DIMENSIONAL DOUBLE-WELL POTENTIAL

Let us consider the following one-dimensional double-well potential:

$$V(x) = \begin{cases} \lambda(x-x_0)^4 - (x-x_0)^2, & x \geqslant x_0, \\ 0, & -x_0 \leqslant x \leqslant x_0, \\ \lambda(x+x_0)^4 - (x+x_0)^2, & x \leqslant -x_0, \end{cases} \tag{5}$$

with $\lambda, x_0 > 0$. We can separately tune the width and the height of the barrier, varying λ and x_0. The height of the energy barrier is $\Delta V = 1/4\lambda$, and the distance between the two minima is $d = 2(x_0 + \sqrt{1/2\lambda})$ (see the inset of Fig. 3). Decreasing λ reduces the energy splitting Δ, as the two wells become deeper and more separated. The parameter x_0 only increases the well separation but does not change the potential energy barrier height. Moreover, a variation of x_0 leaves the characteristic frequency of the potential wells unchanged, i.e., the kinetic energy associated with the localized states $|\psi_L\rangle$ and $|\psi_R\rangle$.

Following Ref. [27], we measure the mean first tunneling time (MFTT), defined as the number of updates required to find the system in the right well, if the particle has been localized in the left one at the beginning of the simulation. From Fig. 3 we see that the MFTT scales as $1/\Delta^2$ when PBCs are used, whereas it scales as $1/\Delta$ for OBCs, as the parameters x_0 and λ change. The gap Δ is obtained using a discrete variable representation (DVR) technique [43]. This scaling relation

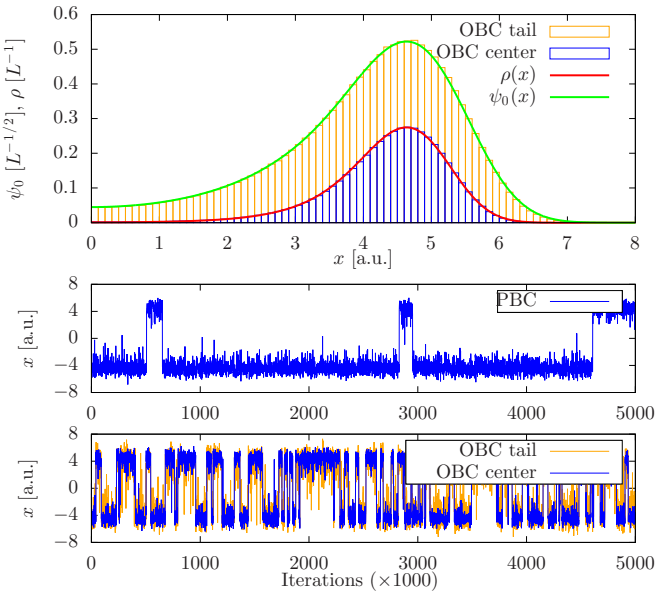

FIG. 4. Top panel: position distributions (histograms) obtained considering the center (blue) or the tail (orange) of the OBC path. The distributions are area-normalized, respectively, with the exact $\rho(x) \approx |\psi_0|^2$ distribution (red) and the exact ground state $\psi_0(x)$ (green). We plot only for $x > 0$ and we use $x_0 = 3$ and $\lambda = 0.14$ in Eq. (5). The difference between the sampled distributions and the reference ones are negligible. We perform simulations at low temperatures, $\beta = 20 \gg \Delta V$. Middle and lower panel: the position of the particle as the simulation progresses for PBCs and OBCs (both for the center and the tail). As expected, the tunneling rate is much larger for OBCs.

holds for PIMC with local METROPOLIS updates and PIMD (using both first- and second-order Langevin thermostats), at large β, and in the limit of small time steps δ_τ, δ_t(for PIMD) $\rightarrow$ 0 limit. This means that the scaling of the tunneling rate in a double-well model, $k \propto \Delta^2$, is correctly reproduced [19]. Since the computational time required to evaluate tunneling splittings increases as the gaps become smaller, we limit the present simulations to a finite set of potential parameters, which allow us to acquire sufficient MFTT statistics.

Why do the open paths tunnel faster from the point of view of PIMC pseudodynamics? To answer this question, we first observe that, for sufficiently low temperatures, the center of the open path $\mathbf{x}^*(\tau \approx \beta/2)$ sample from the ground-state distribution $|\psi_0(x)|^2$, whereas the tails, $\mathbf{x}^*(\tau \approx 0)$ and $\mathbf{x}^*(\tau \approx \beta)$, sample from the ground-state distribution $\psi_0(x)$. Therefore, the tails spend more time inside the barrier (see Fig. 4) compared to the center, which follows instead the more localized ψ_0^2 distribution. Once one of the two tails crosses the barrier, then the rest of the open polymer may easily follow, so that the whole polymer "tunnels" faster compare to its PBC counterpart. This also means that, with OBC, it is possible to sample from the equilibrium distribution $\rho(x) \approx |\psi_0|^2$, using the center of the path, while having a considerable speedup in the sampling. We notice that this feature is not surprising as the OBC technique is closely related to the so called *path integral ground state* [44] (PIGS) technique. Indeed, in the PIGS [44] approach, sampling from the tails gives the mixed distribution $\psi_0(x)\psi_T(x)$, but in our case the trial wave function is $\psi_T(x) = 1$.

Therefore, we propose that OBCs should be used not only in the context of quantum annealing but much more broadly also in material simulations, as far as low-temperature conditions are investigated.

IV. MULTIDIMENSIONAL TUNNELING

The double-well model provided in Sec. III is a prototypical example of one-dimensional tunneling. One could argue that, despite having many-spin degrees of freedom, the spin models investigated in Ref. [27] are also effectively one-dimensional models, as the relevant reaction coordinate is the total scalar magnetization M. Indeed, the *instantonic* nature of the transition state can be seen if we plot $M(\tau)$ as a function of the imaginary-time parameter τ.

It is much more straightforward to devise models that require multidimensional tunneling in continuous space, rather than spin models [45,46]. Toward that end, we borrow insights from quantum chemistry, where simplified model for characterizing proton tunneling have been devised [4,28,47,48]. In particular, in Ref. [28] a semiclassical theory of multidimensional tunneling is formulated, unraveling its qualitative differences compared to one-dimensional tunneling. It was found that in multidimensional tunneling, two regimes can be identified: the *pure tunneling* case, which is effectively one-dimensional, where the tunneling path can be defined uniquely, and the *mixed tunneling* regime, when tunneling occurs very broadly, i.e., where a set of dominant semiclassical paths $\{\mathbf{x}_{\mathrm{TS}}\}$ is not defined. In the first case, the action that defines the semiclassical wave function is purely imaginary, whereas in the latter the action is complex. We refer the interested reader to Ref. [28] for analytical details.

Investigating QMC simulations for such mixed tunneling models, where the QMC scaling relation with the exact QMT rate might be expected to break down, we instead find that the quantum tunneling rate given by QMC scales as the adiabatic quantum evolution also in this case.

A. QMC tunneling rate scaling

We first consider the simple *shifted parabola* bidimensional model of Ref. [28], which is a minimal model for the antisymmetric mode coupling mechanism for proton tunneling in malonaldehyde, a well-studied molecular test case. The Hamiltonian reads

$$H = \Theta + V_A, \tag{6}$$

with

$$\Theta = -\frac{g^2}{2}\left(\frac{\partial^2}{\partial x^2} + \frac{\partial^2}{\partial y^2}\right), \tag{7}$$

where $g > 0$ is a dimensionless parameter that sets the strength of the quantum fluctuations. The potential is

$$V_A(x,y) = \begin{cases} \frac{1}{2}(x+1)^2 + \frac{1}{2}\omega_y^2(y+y_0)^2, & x < 0, \\ \frac{1}{2}(x-1)^2 + \frac{1}{2}\omega_y^2(y-y_0)^2, & x \geqslant 0, \end{cases} \tag{8}$$

where $y_0 \geqslant 0$ and $\omega_y^2 > 0$ are dimensionless harmonic potential parameters. This potential represents two parabolas,

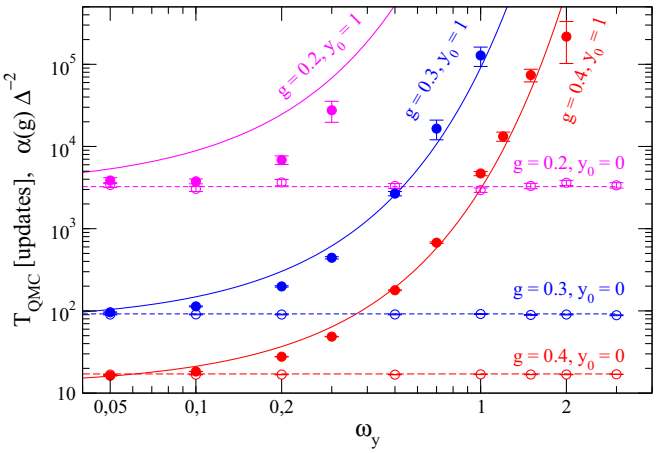

FIG. 5. Average MFTT tunneling time with PIMC (with PBC) as a function of ω_y for different values of $g = 0.2,0.3,0.4$ (pink, blue, and red data series, respectively) and two values of $y_0 = 0$ (empty symbols) and 1 (full symbols). The potential considered is V_A as in Eq. (8). Lines represent a fit to the exact Δ^{-2} gap values, obtained with the DVR method. The proportionality constant $\alpha(g)$ that multiplies the inverse gap squared is different for each g value, and it is fitted using only the $y_0 = 0$ data series. Notice the logarithmic scale on both axes.

located, respectively, in the half-planes $x < 0$ and $x > 0$, with centers shifted along the y axis by an amount $2y_0$. In the case of a malonaldehyde molecule, the coordinate x represents the motion of transferring the proton, while y represents the C-O stretching mode.

Following Ref. [28], let us introduce a parameter $a^2 = y_0^2 - g/\omega_y$, whose sign distinguishes between the two ground-state QMT cases: pure tunneling for $a^2 > 0$ and mixed tunneling for $a^2 < 0$.

In Fig. 5 we present results of PIMC simulations with local updates, using PBC, at large β (very low temperature), and in the converged time step $\delta_\tau \to 0$ limit, to describe faithfully ground-state tunneling. The path deformations are obtained by displacing each bead at a time by an amount (dx,dy). The displacements are Gaussian-distributed with zero mean, and the variance is tuned in order to obtain a METROPOLIS acceptance probability of ≈40%.

Again we study the MFTT obtained with PIMC simulations as a function of the parameter ω_y, in the range $[0.05,2]$ and for three different choices of $g = 0.2,0.3,0.4$, and for two shifting values $y_0 = 0$ and 1. Following Ref. [27], we define the MFTT as the number of PIMC updates required to observe an instantonic state. In turn, we algorithmically define an instanton path as spending approximately the same fraction of imaginary time in either well.

With these parameter ranges,[1] we can roughly mimic proton transfer reactions in malonaldehyde [48]. For this molecule, it is found that if the tunneling is described only by a one-dimensional process, the tunneling rate is reduced by two orders of magnitude compared to experimental and recent theoretical values [49,50]. Furthermore, it was argued in Ref. [28] that deviations from the one-dimensional picture lead to a mixed tunneling regime where no well-defined tunneling path exists. Therefore, it could be possible that QMC underestimates the exact tunneling rate. In the context of a quantum annealing problem, this might mean that the performances of QA and its simulated version through QMC could be very different, under these "mixed tunneling" conditions.

We first perform tests for $y_0 = 0$. While according to Ref. [28] we are in the mixed tunneling regime, in this case x and y directions decouple, leading with effective one-dimensional tunneling along the x direction. Indeed, the gap Δ is constant as a function of ω_y, and we observe the same in QMC, where the MFTT remains constant. Its precise value depends on the parameter g. We use these data to fix the proportionality constant $\alpha(g)$, which we use later to compare the MFTT to the value $\alpha(g)\Delta^{-2}$. Notice that in the $\omega_y \to 0$ limit the two wells become parallel and indefinitely extended along the y direction. In this limit, we observe an *infinite* number of tunneling paths that connect reactants on the left well with the products on the right.

Next, we set $y_0 = 1$ and repeat the simulations. This time the scaling of Δ^{-2} as a function of ω_y is nontrivial. Nevertheless, it approaches the previous value—for any given g—in the $\omega_y \to 0$ limit, as the two wells are infinitely long and the shift given by y_0 becomes irrelevant. In this case, we cross the transition point $a^2 = 0$ between the two regimes of tunneling, when $\omega_y = g$. We observe a satisfactory agreement between the QMC MFTT data series and the $\alpha(g)\Delta^{-2}$ functions, while residual differences still remain. Notice also that, if we fix the constant $\alpha(g)$ targeting the pure tunneling regime, then the QMC tunneling time is always slightly smaller than $\alpha(g)\Delta^{-2}$, so QMC seems to be slightly more efficient than QA, even with PBC.

B. QMC reaction pathways and fluctuations around the instanton solution

In this section, we explicitly track the QMC pseudodynamics transition states and compare to the instantonic trajectory computed by minimizing the action S. Let us consider the *symmetric* mode coupling potential,

$$V_S(x,y) = \frac{1}{8}(x-1)^2(x+1)^2 + \frac{\omega_y^2}{2}\left(y + \frac{\gamma}{\omega_y^2}(x^2+1)\right)^2. \tag{9}$$

This potential energy surface is continuous and has been widely used as a model for proton tunneling. In the typical example of malonaldehyde, the coordinate x represents the motion of the proton transferring between the oxygen atoms, while y gives the scissorslike motion of the O-C-C-C-O frame [28]. We use the dimensionless potential parameters $(\omega_y,\gamma,g) = (0.48,0.39,0.10)$ to fit the model to the *ab initio* potential energy surface [49]. In this way, we can directly compare the transition paths given by the PIMC simulation with other techniques, such as the *ring polymer instanton* (RPI) method [6,50–52], recently introduced to calculate energy splitting. In the RPI framework, one first needs to locate the saddle point of the action S (the instanton), and then evaluate

[1]The actual value would be $g \approx 0.1$; here, we artificially enhance $\hbar$ in order to increase the observed tunneling rate.

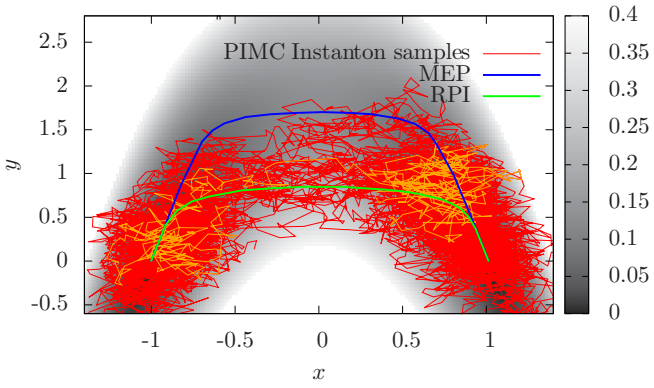

FIG. 6. Heat-map plot of the two-dimensional model potential $V_S(x,y)$ of malonaldehyde of Eq. (9). Red lines represents a collection of 20 instanton paths sampled with PIMC. These samples are uncorrelated as they correspond to independent tunneling events after full reinitialization of the starting path in the reactant well. That is, when the MFTT identification criteria are met (see the text), we stop the PIMC simulation and collect the last path that has been generated. We use a sufficiently large inverse temperature ($\beta = 400$, $P = 512$), Trotter slices, and OBCs in imaginary time. We single out, in orange, one of these instances in order to appreciate their *instantonic* character. Indeed, most of the Trotter slices are located at the bottom of the two wells, and only a very few of them are located on the barrier (cf. Fig. 2); these correspond to the middle of the imaginary-time trajectory ($\tau \approx \beta/2$). The PIMC instanton paths are not smooth, given the large number of Trotter slices, and they represent fluctuations around an average transition path that is qualitatively very close to the RPI solution taken from Ref. [50] (green; see the text). We also plot the MEP (blue) for comparison. The proton tunneling paths typically take place on a region quite far from the saddle point ($0, \gamma/\omega_y^2 \approx 1.7$) of the potential.

the splitting energy by computing the functional integral up to second order in the fluctuations around the dominant contribution. This approach employs neither PIMC sampling nor PIMD, as the instanton path is obtained via the action's minimization and the initial guess is an OBC path that already connects the reactant to the product state.

In Fig. 6, we plot a sample of transition paths produced by the PIMC pseudodynamics, and we recognize their instantonic character. We compare some OBC transition paths sampled with our PIMC simulation against the RPI solution recently published in Ref. [50]. We see that these instanton paths form a bundle around the RPI saddle point solution, and they are qualitatively distant from the minimum energy path (MEP), which would be typical of a classical thermally activated process [50]. It is remarkable that a simple PIMC simulation obtains the instanton path, which is otherwise computed only by a complex minimization procedure as in the RPI scheme.

Another advantage of PIMC is that we can directly sample the statistical fluctuations around the dominant solution $\mathbf{x}^*(\tau)$. To second order, the action can be expanded as [35]

$$S \simeq S[\mathbf{x}^*] + \frac{1}{2}\int_0^\beta d\tau' \int_0^\beta d\tau'' \frac{\delta^2 S[\mathbf{x}^*]}{\delta \mathbf{x}(\tau')\delta \mathbf{x}(\tau'')}\mathbf{y}(\tau)\mathbf{y}(\tau)$$
$$\simeq S[\mathbf{x}^*] + \frac{1}{2}\int_0^\beta d\tau\, \mathbf{y}(\tau)\hat{G}[\mathbf{x}^*]\mathbf{y}(\tau), \qquad (10)$$

where $\mathbf{y}(\tau)$ is a fluctuation path, satisfying $\mathbf{y}(0) = \mathbf{y}(\beta) = \mathbf{0}$, and $\hat{G} = -\frac{d^2}{d\tau^2} + V''[\mathbf{x}^*]$ is the fluctuation operator, or Hessian, adopting the notation of Ref. [51]. Here $V''[\mathbf{x}^*]$ is the second derivative of the potential computed along the instanton path $\mathbf{x}^*(\tau)$.

In practice, one always deals with discretized trajectories in imaginary time. Therefore, also the operator $\hat{G}$ is discretized using finite differences and then diagonalized to obtain the normal modes and frequency of the fluctuations. The resulting product of Gaussian integrals allows one to evaluate Eq. (10).

However, it could be cumbersome to evaluate G for *ab initio* potentials (as they require an evaluation of the second derivatives of the potential), or in the case of rugged energy landscapes, where local curvature at the saddle point $V''[\mathbf{x}^*]$ does not correctly represent the actual amplitude of the quantum fluctuations [38,53]. On the other hand, the inverse operator G^{-1} can be computed stochastically with PIMC, using the relation

$$\hat{G}^{-1}[\mathbf{x}^*](\tau_1,\tau_2) = \langle \mathbf{y}(\tau_1)\mathbf{y}(\tau_2)\rangle_{\mathbf{x}^*}, \qquad (11)$$

where the right-hand side denotes the statistical average of the fluctuations, around a given path $\mathbf{x}^*$. This approach gives a more effective and fast estimate of the curvature of the potential surface in the above cases.

We note that PIMC sampling techniques have already been used to compute tunneling splittings in molecular and condensed-matter systems [54–57]. Here we propose an alternative and simple way to compute ratios of quantum-mechanical rate constants. Suppose that the potential displays several minima, i.e., that we have one reactant state R and two or more possible product states P_1, P_2. By computing the ratio of the average PIMC tunneling times with OBCs, required to perform the transitions $R \to P_1$ and $R \to P_2$, respectively, we can estimate the ratio of the tunneling splittings $\Delta_{R,P_2}/\Delta_{R,P_1}$ corresponding to the two quantum-mechanical transitions, provided that enough statistics of instanton events can be gathered in a reasonable amount of time. This approach is predictive, as the instantons are generated by the PIMC pseudodynamics without any *a priori* knowledge of the final product state.

This problem is closely connected with quantum annealing, where, starting from some high-energy "reactant" states R's, one would like to reach the "product" state P_i having the lowest possible potential energy after a sequence of tunneling events [58]. The relative probability of finding this state, compared to other metastable ones, is well described by PIMC simulations.

V. POTENTIAL OBSTRUCTIONS FOR QMC SIMULATIONS

While the above results hold in a broad class of spin and continuous models, let us list here also possible counterexamples to this finding, where obstructions to efficient QMC simulations are present. The first kinds of counterexamples are models in which *topological* obstructions for a PBC path integral exist. In these cases, the paths cannot explore all the space because local updates cannot generate paths having different winding-numbers [59,60]. On the other hand, global updates can easily restore ergodicity in all cases, but at the expense of generating *instantonlike* moves and therefore

biasing the MFTT estimation. Nevertheless, this issue may be solved by using OBCs instead of PBCs.

A different type of obstruction is realized in models in which the wave function and its square modulus are concentrated on different supports [59,61]. This obstruction remains even in the OBC approach. Indeed, the tails (which sample from the ground state) and the center (which samples from its square) may remain trapped in different subspaces, breaking the ergodicity of the simulations. We notice that examples that display such features are *ad hoc* designed discrete models, and it would be extremely interesting to find counterparts in realistic continuous-space models.

Finally, we remark that a practical limitation of this technique concerns the evaluation of vanishingly small gaps. Indeed, the waiting time to observe instantons in PIMC increases as the tunneling splitting become smaller. So even if QMC only requires polynomially increasing resources to simulate the system, if the gap closes exponentially with the system size, the QMC simulation time will also increase exponentially.

VI. CONCLUSIONS

We have studied the tunneling of path-integral-based equilibrium simulations in continuous-space models, generalizing a previous study [27] on ferromagnetic spin models. We demonstrate that the PIMC tunneling rate scales as a Δ^2 if periodic boundary conditions in imaginary time are used, while it scales as Δ with open boundary conditions. These scaling relations seem to be a general property of path integral methods, as long as reasonable semilocal updates are employed during the Markov chain pseudodynamics (see Sec. II B). In this case, in double-well potentials, it is possible to directly identify the transition state of the path integral pseudodynamics—a purely classical process—and therefore compute its classical reaction rate using Kramers theory.

This transition state is the *instanton* path, and we remark here that this trajectory is sampled by the PIMC pseudodynamics using local updates, i.e., we do not need to engineer such global update moves as in Refs. [45,56]. Indeed, the latter approach would invalidate the premises and discussions presented in this paper and artificially increase the reaction rate observed with PIMC. On the other hand, building in instantonic updates in the METROPOLIS procedure requires full knowledge of the system, i.e., knowing in advance the transition states. Having this knowledge, one would solve beforehand the quantum annealing problem, for example, without even running any PIMC simulation.

We remark again that what we found concerns the *scaling* of the quantum tunneling splitting. It is not possible to determine quantitatively the quantum rate with a single-shot simulation yet. Indeed, while the exponent of the QMC tunneling rate (i.e., the inverse of the MFTT) is not sensitive to the specific choice of the updates in the QMC pseudodynamics, the QMC prefactor depends on the details of the simulation. For this reason, only the ratio of two tunneling splittings can be calculated using the present technique, as discussed in Sec. IV B.

The quadratic speed-up in tunneling efficiency is a robust feature of OBC simulations for tunneling through individual barriers. In the context of simulations, therefore, we propose that open path integral simulations should be used instead of PBCs and will accelerate the sampling whenever ground-state properties are desired.

We also turned our attention to simplified models for proton transfer, where multidimensional tunneling is deemed important, and a semiclassical description of tunneling as an effective one-dimensional process has been seen to fail. Nevertheless, the scaling relation of the PIMD transition rate, compared to the exact incoherent tunneling rate Δ^2, holds also in this case.

The above finding is very interesting because often in a multidimensional potential the smooth tunneling path (instanton) connecting the minima of the potential does not exist due to the effects of so-called dynamical tunneling [28,62–64]. The lack of an instanton path was also studied, e.g., in the case of the two-dimensional shifted parabola model [28] considered in our study. On the other hand, as explained above in Sec. II B based on the Kramers theory arguments, the existence of the instanton path is a key requirement that leads to identical QMT and PIMC scaling laws.

To explain this conundrum, we observe that the difficulty with an instanton description in the case of tunneling in a multidimensional potential usually occurs when one needs to match the solutions given by Wentzel-Kramers-Brillouin (WKB) theory in classically allowed and forbidden regions at the boundary formed by caustics. Caustics result in the complex (oscillatory) behavior of the wave function under the barrier [28,62,63]. This oscillatory behavior results in a phase problem in QMC.

We argue that at zero temperature this situation does not occur generically, because a classically allowed region in configuration space "collapses" into the point corresponding to the minimum of the potential. As usual, to study tunneling one should consider the wave function under the barrier that nearly coincides with the ground-state wave function near one of the minima of V, exponentially decaying away from it. The mechanical action $S[\mathbf{x}(\tau)] = \int_{\infty}^{\tau}[m\dot{\mathbf{x}}^2(\tau_1) + V(\mathbf{x}(\tau_1))]d\tau_1$ for the wave function is associated with the unstable Lagrangian manifold [65] formed by real-valued trajectories $(\mathbf{x}(\tau),\mathbf{p}(\tau))$ in the phase space moving in the imaginary time τ in the inverted potential $-V$ [above $\mathbf{p}(\tau)$ is a system momentum]. The trajectories emanate at time $t = -\infty$ from the corresponding maximum of the $-V$. In general, projections of the Lagrangian manifold onto the coordinate space $\mathbf{x}$ can have caustics and cusps (and more complex singularities in dimensions higher than 2 [66]) in the classically forbidden region. These singularities lead to multivaluedness of the action surface, and some of its branches become complex. However, the *minimum action* surface is real- and single-valued. It possesses lines where the surface gradient is discontinuous (see Fig. 7). They correspond to the so-called switching lines in configuration space [67]. Points at different sides of the switching are reached by topologically different imaginary-time paths, as shown in Fig. 7(b). Therefore, any point $\mathbf{x}$ can be reached by the most probable path that provides the minimum of the action and never crosses a switching line. An instanton is a particular member of the minimum-action family of paths that connects the two maxima of the potential $-V$. It corresponds to the heteroclinic orbit $(\mathbf{x}^*(\tau),\mathbf{p}^*(\tau))$ contained

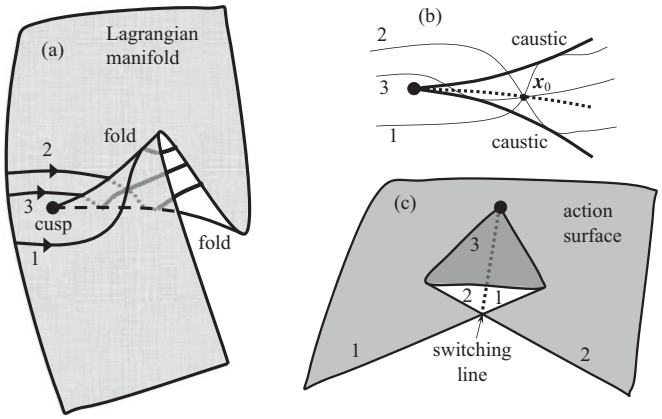

FIG. 7. (a) Unstable manifold with a cusp singularity and three typical imaginary-time paths emanating from one of the minima of the potential. (b) Projection of the unstable manifold onto the coordinate plane (X_1, X_2). The two folds project onto caustics, while projections of the three trajectories intersect at the point X_0 that lies on the switching line, showed as a dashed line. (c) The action $S(X_0)$ is a three-valued function in between the caustics. Two of its lower branches intersect along the switching line. After Refs. [67,69].

in the unstable Lagrangian manifold shared by the two maxima [68]. This explains why ground-state tunneling splitting for the particle in a multidimensional potential is always described by the instanton with a real-valued action and therefore can be simulated efficiently by PIMC.

This confirms that PIMC simulation of QMT in the ground state can be done without any loss of efficiency compared to what a real system would do. The fact that PIMC simulations have the same scaling with the problem size as physical quantum annealing was recently confirmed experimentally, again on a spin system on a chimera graph [70]. In this context, it is unlikely that QA will find a ground state of optimization problem that can achieve an exponential speedup over classical computation only by using QMT as a computational resource.

We remark here that these conclusions hold only when so-called *stoquastic* Hamiltonians are used, i.e., Hamiltonians that allow PIMC simulations. This is the case of the Hamiltonians used in this paper. In most reaction simulations, protons are assumed to be distinguishable particles, and in QA the standard transverse field Ising Hamiltonian is also *stoquastic* [11,12]. This provides additional evidence that QA machines should implement *nonstoquastic* Hamiltonians that display a sign problem [71–73] in order to avoid efficient simulations by QMC methods.

ACKNOWLEDGMENTS

G.M. acknowledges useful discussions with P. Faccioli, S. Sorella, and G. E. Santoro. M.T. acknowledges the hospitality of the Aspen Center for Physics, supported by NSF Grant No. PHY-1066293. Simulations were performed on resources provided by the Swiss National Supercomputing Centre (CSCS). This work was supported by the European Research Council through ERC Advanced Grant SIMCOFE by the Swiss National Science Foundation through NCCR QSIT and NCCR Marvel. This paper is based upon work supported in part by ODNI, IARPA via MIT Lincoln Laboratory Air Force Contract No. FA8721-05-C-0002. The views and conclusions contained herein are those of the authors and should not be interpreted as necessarily representing the official policies or endorsements, either expressed or implied, of ODNI, IARPA, or the US Government. The US Government is authorized to reproduce and distribute reprints for Governmental purpose notwithstanding any copyright annotation thereon.

APPENDIX: DETAILS OF THE PATH INTEGRAL SIMULATIONS

The typical Hamiltonian (here written in one dimension for the sake of simplicity) is given by

$$H = \frac{p^2}{2m} + V(x), \tag{A1}$$

where x and p are the position and momentum coordinate, respectively, m is the mass of the particle, and $V(x)$ is the potential. The kinetic operator is $p^2/2m$, where the strength of the quantum fluctuations is controlled by the particle's mass m. By applying the standard Trotter breakup for the density operator $e^{-H/T}$, the partition function at temperature T is given by

$$Z = \mathrm{tr}\, e^{-H/T} \approx \int dx \exp\left[-\sum_{k=1}^{P} \left(\frac{mPT}{2}(x_k - x_{k+1})^2 + \frac{1}{PT} V(x_k) \right) \right], \tag{A2}$$

where x_k is the coordinate of the kth system's replica (time slice), and P is the total number of Trotter replicas. If we use PBC, then $x_{P+1} = x_1$. We refer the reader to Ref. [21] for additional details concerning energy estimators and more sophisticated Trotter breakups, i.e., more accurate approximate propagators. Equation (A2) represents the partition function of a classical ring polymer, made of P beads at the fictitious temperature PT. The neighboring replicas (in imaginary time) interact via a harmonic potential having a spring constant $\kappa = m(PT)^2$.

PIMC. The simplest way to sample Z is to perform METROPOLIS Monte Carlo moves on this extended system, the METROPOLIS weight being the integrand of Eq. (A2). The simplest local update consists in moving only one coordinate replica $x_k' \to x_k + \delta z$ and accepting/rejecting the move according to the METROPOLIS algorithm. z is a uniform random number in the range $[-1,1]$, and δ is tuned in order to optimize the autocorrelation times. This is the kind of local update used in the main text. One MC sweep consists of P local attempts.

PIMD. It is possible to sample from the finite-temperature canonical distribution of the ring polymer [74] using also molecular dynamics (MD). In this case, the sampling is driven by the forces. Among all the possible MD integrator schemes, here we choose the Langevin equation of motions. Two kinds of Langevin MD can be considered, namely *first* and *second* order. The first-order case can be considered as a particular case of PIMC where the updates are not completely random,

i.e., they follow the forces, and where the acceptance/rejection is missing. In this case, the update rule consists in

$$x'_k = x_k + \delta f_k + \sqrt{2T\delta}\eta_k, \tag{A3}$$

where δ is the integration time step, η is a Gaussian-distributed random number (with zero mean and unitary variance), and f_k includes all the forces acting on the kth replicas,

$$f_k = -\frac{\partial V(x_k)}{\partial x_k} \Big/ P + PT^2 m(x_{k+1} - 2x_k + x_{k-1}). \tag{A4}$$

In the MD framework, all updates are accepted at the cost of introducing a time-step discretization error, which can be systematically removed in the limit $\delta \to 0$.

In the second-order case, we instead add the conjugate momenta π to the x coordinates, so that the ring polymer Hamiltonian reads

$$H_{\rm cl} = \sum_{k=1}^{P} \left(\frac{\pi_k^2}{2} + \frac{m(PT)^2}{2}(x_k - x_{k+1})^2 + \frac{1}{PT} V(x_k) \right).$$

To sample the equilibrium distribution $e^{-H_{\rm cl}/PT}$, we integrate the following equation of motion:

$$\pi'_k = (1 - \delta\gamma)\pi_k + \delta/m f_k + \sqrt{2\gamma T\delta/m}\eta, \tag{A5}$$

$$x'_k = x_k + \pi_k \delta, \tag{A6}$$

where, again, δ is the integration time step, η is a Gaussian-distributed random number, and f_k includes all the forces acting on the kth replicas. In this equation, γ is a parameter that has to be tuned in order to minimize autocorrelation times and—in general—can also be position-dependent.

[1] Z. D. Nagel and J. P. Klinman, Tunneling and dynamics in enzymatic hydride transfer, Chem. Rev. **106**, 3095 (2006).

[2] R. P. Bell, *The Tunnel Effect in Chemistry* (Chapman and Hall, London, 1980).

[3] P. S. Zuev, R. S. Sheridan, T. V. Albu, D. G. Truhlar, D. A. Hrovat, and W. T. Borden, Carbon tunneling from a single quantum state, Science **299**, 867 (2003).

[4] H. Nakamura and G. Mil'nikov, *Quantum Mechanical Tunneling in Chemical Physics* (CRC, Boca Raton, FL, 2013).

[5] M. Ceriotti, W. Fang, P. G. Kusalik, R. H. McKenzie, A. Michaelides, M. A. Morales, and T. E. Markland, Nuclear quantum effects in water and aqueous systems: Experiment, theory, and current challenges, Chem. Rev. **116**, 7529 (2016).

[6] J. O. Richardson, C. Pérez, S. Lobsiger, A. A. Reid, B. Temelso, G. C. Shields, Z. Kisiel, D. J. Wales, B. H. Pate, and S. C. Althorpe, Concerted hydrogen-bond breaking by quantum tunneling in the water hexamer prism, Science **351**, 1310 (2016).

[7] S. A. Bonev, E. Schwegler, T. Ogitsu, and G. Galli, A quantum fluid of metallic hydrogen suggested by first-principles calculations, Nature (London) **431**, 669 (2004).

[8] C. J. Pickard and R. J. Needs, Structure of phase III of solid hydrogen, Nat. Phys. **3**, 473 (2007).

[9] P. Dalladay-Simpson, R. T. Howie, and E. Gregoryanz, Evidence for a new phase of dense hydrogen above 325 gigapascals, Nature (London) **529**, 63 (2016).

[10] G. Mazzola and S. Sorella, Accelerating *ab initio* Molecular Dynamics and Probing the Weak Dispersive Forces in Dense Liquid Hydrogen, Phys. Rev. Lett. **118**, 015703 (2017).

[11] M. W. Johnson, M. H. S. Amin, S. Gildert, T. Lanting, F. Hamze, N. Dickson, R. Harris, A. J. Berkley, J. Johansson, P. Bunyk, *et al.*, Quantum annealing with manufactured spins, Nature (London) **473**, 194 (2011).

[12] P. I. Bunyk, E. M. Hoskinson, M. W. Johnson, E. Tolkacheva, F. Altomare, A. J. Berkley, R. Harris, J. P. Hilton, T. Lanting, A. J. Przybysz, and J. Whittaker, Architectural considerations in the design of a superconducting quantum annealing processor, IEEE Trans. Appl. Supercond. **24**, 1 (2014).

[13] E. Farhi, J. Goldstone, S. Gutmann, and M. Sipser, Quantum computation by adiabatic evolution, arXiv:quant-ph/0001106.

[14] T. Kadowaki and H. Nishimori, Quantum annealing in the transverse Ising model, Phys. Rev. E **58**, 5355 (1998).

[15] E. Farhi, J. Goldstone, S. Gutmann, J. Lapan, A. Lundgren, and D. Preda, A quantum adiabatic evolution algorithm applied to random instances of an NP-complete problem, Science **292**, 472 (2001).

[16] A. Das and B. K. Chakrabarti, Colloquium: Quantum annealing and analog quantum computation, Rev. Mod. Phys. **80**, 1061 (2008).

[17] E. Crosson and A. W. Harrow, Simulated quantum annealing can be exponentially faster than classical simulated annealing, in *IEEE 57th Annual Symposium on Foundations of Computer Science (FOCS)* (IEEE, Piscataway, NJ, 2016), pp. 714–723.

[18] S. Boixo, V. N. Smelyanskiy, A. Shabani, S. V. Isakov, M. Dykman, V. S. Denchev, M. H. Amin, A. Y. Smirnov, M. Mohseni, and H. Neven, Computational multiqubit tunneling in programmable quantum annealers, Nat. Commun. **7**, 10327 (2016).

[19] U. Weiss, H. Grabert, P. Hänggi, and P. Riseborough, Incoherent tunneling in a double well, Phys. Rev. B **35**, 9535 (1987).

[20] B. J. Berne and D. Thirumalai, On the simulation of quantum systems: Path integral methods, Annu. Rev. Phys. Chem. **37**, 401 (1986).

[21] D. M Ceperley, Path-integrals in the theory of condensed helium, Rev. Mod. Phys. **67**, 279 (1995).

[22] M. Ceriotti, J. Cuny, M. Parrinello, and D. E Manolopoulos, Nuclear quantum effects and hydrogen bond fluctuations in water, Proc. Natl. Acad. Sci. (USA) **110**, 15591 (2013).

[23] J. A. Morrone and R. Car, Nuclear Quantum Effects in Water, Phys. Rev. Lett. **101**, 017801 (2008).

[24] J. Chen, X.-Z. Li, Q. Zhang, M. I. J. Probert, C. J Pickard, R. J. Needs, A. Michaelides, and E. Wang, Quantum simulation of low-temperature metallic liquid hydrogen, Nat. Commun. **4**, 2064 (2013).

[25] G. E. Santoro, R. Martonak, E. Tosatti, and R. Car, Theory of quantum annealing of an Ising spin glass, Science **295**, 2427 (2002).

[26] B. Heim, T. F. Rønnow, S. V. Isakov, and M. Troyer, Quantum versus classical annealing of Ising spin glasses, Science **348**, 215 (2015).
[27] S. V. Isakov, G. Mazzola, V. N. Smelyanskiy, Z. Jiang, S. Boixo, H. Neven, and M. Troyer, Understanding Quantum Tunneling Through Quantum Monte Carlo Simulations, Phys. Rev. Lett. **117**, 180402 (2016).
[28] S. Takada and H. Nakamura, Wentzel-Kramers-Brillouin theory of multidimensional tunneling: General theory for energy splitting, J. Chem. Phys. **100**, 98 (1994).
[29] J. Cao and G. A. Voth, A new perspective on quantum time correlation functions, J. Chem. Phys. **99**, 10070 (1993).
[30] I. R. Craig and D. E. Manolopoulos, Quantum statistics and classical mechanics: Real time correlation functions from ring polymer molecular dynamics, J. Chem. Phys. **121**, 3368 (2004).
[31] S. Jang, A. V. Sinitskiy, and G. A. Voth, Can the ring polymer molecular dynamics method be interpreted as real time quantum dynamics? J. Chem. Phys. **140**, 154103 (2014).
[32] B. J. Braams and D. E. Manolopoulos, On the short-time limit of ring polymer molecular dynamics, J. Chem. Phys. **125**, 124105 (2006).
[33] T. J. H. Hele, M. J. Willatt, A. Muolo, and S. C. Althorpe, Communication: Relation of centroid molecular dynamics and ring-polymer molecular dynamics to exact quantum dynamics, J. Chem. Phys. **142**, 191101 (2015).
[34] Z. Jiang, V. N. Smelyanskiy, S. V. Isakov, S. Boixo, G. Mazzola, M. Troyer, and H. Neven, Scaling analysis and instantons for thermally assisted tunneling and quantum Monte Carlo simulations, Phys. Rev. A **95**, 012322 (2017).
[35] G. Parisi and Y.-S. Wu, Perturbation theory without gauge fixing, Sci. Sin. **24**, 483 (1981).
[36] M. Sega, P. Faccioli, F. Pederiva, G. Garberoglio, and H. Orland, Quantitative Protein Dynamics from Dominant Folding Pathways, Phys. Rev. Lett. **99**, 118102 (2007).
[37] E. Autieri, P. Faccioli, M. Sega, F. Pederiva, and H. Orland, Dominant reaction pathways in high-dimensional systems, J. Chem. Phys. **130**, 064106 (2009).
[38] G. Mazzola, S. a Beccara, P. Faccioli, and H. Orland, Fluctuations in the ensemble of reaction pathways, J. Chem. Phys. **134**, 164109 (2011).
[39] S. Coleman, Fate of the false vacuum: Semiclassical theory, Phys. Rev. D **15**, 2929 (1977).
[40] H. Forkel, A primer on instantons in QCD, arXiv:hep-ph/0009136.
[41] E. M. Chudnovsky and J. Tejada, *Macroscopic Quantum Tunneling of the Magnetic Moment* (Cambridge University Press, Cambridge, 1998).
[42] P. Hänggi, P. Talkner, and M. Borkovec, Reaction-rate theory: Fifty years after Kramers, Rev. Mod. Phys. **62**, 251 (1990).
[43] D. T. Colbert and W. H. Miller, A novel discrete variable representation for quantum mechanical reactive scattering via the *S*-matrix Kohn method, J. Chem. Phys. **96**, 1982 (1992).
[44] A. Sarsa, K. E. Schmidt, and W. R. Magro, A path integral ground state method, J. Chem. Phys. **113**, 1366 (2000).
[45] L. Stella, G. E. Santoro, and E. Tosatti, Monte Carlo studies of quantum and classical annealing on a double well, Phys. Rev. B **73**, 144302 (2006).
[46] E. M. Inack and S. Pilati, Simulated quantum annealing of double-well and multiwell potentials, Phys. Rev. E **92**, 053304 (2015).
[47] A. Auerbach and S. Kivelson, The path decomposition expansion and multidimensional tunneling, Nucl. Phys. B **257**, 799 (1985).
[48] N. Makri and W. H. Miller, Basis set methods for describing the quantum mechanics of a interacting with a harmonic bath, J. Chem. Phys. **86**, 1451 (1987).
[49] E. Bosch, M. Moreno, J. M. Lluch, and J. Bertrn, Bidimensional Tunneling Dynamics of Malonaldehyde and hydrogenoxalate anion. A comparative study, J. Chem. Phys. **93**, 5685 (1990).
[50] M. T. Cvitas and S. C. Althorpe, Locating instantons in calculations of tunneling splittings: The test case of malonaldehyde, J. Chem. Theor. Comput. **12**, 787 (2016).
[51] J. O. Richardson and S. C. Althorpe, Ring-polymer instanton method for calculating tunneling splittings, J. Chem. Phys. **134**, 054109 (2011).
[52] J. O. Richardson, S. C. Althorpe, and D. J. Wales, Instanton calculations of tunneling splittings for water dimer and trimer, J. Chem. Phys. **135**, 124109 (2011).
[53] P. Faccioli (unpublished).
[54] A. Kuki and P. G. Wolynes, Electron tunneling paths in proteins, Science **236**, 1647 (1987).
[55] D. M. Ceperley and G. Jacucci, Calculation of Exchange Frequencies in bcc ^{3}He with the Path-Integral Monte Carlo Method, Phys. Rev. Lett. **58**, 1648 (1987).
[56] C. Alexandrou and J. W. Negele, Stochastic calculation of tunneling in systems with many degrees of freedom, Phys. Rev. C **37**, 1513 (1988).
[57] E. Mátyus, D. J. Wales, and S. C. Althorpe, Quantum tunneling splittings from path-integral molecular dynamics, J. Chem. Phys. **144**, 114108 (2016).
[58] S. Knysh, Zero-temperature quantum annealing bottlenecks in the spin-glass phase, Nat. Commun. **7** 12370 (2016).
[59] M. B. Hastings, Obstructions to classically simulating the quantum adiabatic algorithm, Quantum Inf. Comput. **13**, 1038 (2013).
[60] E. Andriyash and M. H. Amin, Can quantum Monte Carlo simulate quantum annealing? arXiv:1703.09277.
[61] M. Jarret, S. P. Jordan, and B. Lackey, Adiabatic optimization versus diffusion Monte Carlo methods, Phys. Rev. A **94**, 042318 (2016).
[62] Z. H. Huang, T. E. Feuchtwang, P. H. Cutler, and E. Kazes, Wentzel-Kramers-Brillouin method in multidimensional tunneling, Phys. Rev. A **41**, 32 (1990).
[63] J. Zamastil, Multidimensional wkb approximation for particle tunneling, Phys. Rev. A **72**, 024101 (2005).
[64] M. Razavy, *Quantum Theory of Tunneling*, 2nd ed. (World Scientific, Singapore, 2013).
[65] J. Guckenheimer and P. Holmes, *Nonlinear Oscillations, Dynamical Systems, and Bifurcations of Vector Fields* (Springer, New York, 1983).
[66] V. I. Arnold, *Mathematical Methods of Classical Mechanics* (Springer Verlag, New York, 1978).
[67] M. I. Dykman, M. M. Millonas, and V. N. Smelyanskiy, Observable and hidden singular features of large fluctuations in nonequilibrium systems, Phys. Lett. A **195**, 53 (1994).
[68] T. Sharpee, M. I. Dykman, and P. M. Platzman, Tunneling decay in a magnetic field, Phys. Rev. A **65**, 032122 (2002).

[69] A. Kamenev, *Field Theory of Non-equilibrium Systems* (Cambridge University Press, 2011).

[70] V. S. Denchev, S. Boixo, S. V. Isakov, N. Ding, R. Babbush, V. Smelyanskiy, J. Martinis, and H. Neven, What is the Computational Value of Finite-Range Tunneling? Phys. Rev. X **6**, 031015 (2016).

[71] Y. Seki and H. Nishimori, Quantum annealing with antiferromagnetic fluctuations, Phys. Rev. E **85**, 051112 (2012).

[72] G. Mazzola and M. Troyer, Quantum Monte Carlo annealing with multi-spin dynamics, J. Stat. Mech.: Theor. Exp. (2017) 053105.

[73] L. Hormozi, E. W Brown, G. Carleo, and M. Troyer, Nonstoquastic Hamiltonians and quantum annealing of Ising spin glass, Phys. Rev. B **95**, 184416 (2017).

[74] M. E. Tuckerman, B. J. Berne, G. J. Martyna, and M. L. Klein, Efficient molecular dynamics and hybrid Monte Carlo algorithms for path integrals, J. Chem. Phys. **99**, 2796 (1993).